Journal of Nanoporous Systems

Original Research Paper

Deep Eutectic Solvent-Delaminated Ti_3C_2 MXene for Highly Sensitive Detection of Hydrogen Peroxide

Seyyed Mehdi Khoshfetrat[*1,2]

[1]*Department of Chemistry, Faculty of Basic Sciences, Ayatollah Boroujerdi University, Boroujerd, Iran.*
[2]*Biosensor and Energy Research Center, Ayatollah Boroujerdi University, Boroujerd, Iran.*

Article history
Received: 4 November 2025
Revised: 26 December 2025
Accepted: 3 January 2026

*Corresponding Author:
Seyyed Mehdi Khoshfetrat
Ayatollah Boroujerdi University, Boroujerd, *Iran.*

Email:
*m.khoshfetrat@gmail.com;
sm.khoshfetrat@abru.ac.ir.

Abstract: Hydrogen peroxide (H_2O_2) is a vital oxidizing and signaling molecule extensively used across biomedical, environmental, and industrial fields. Accurate and rapid quantification of H_2O_2 is crucial for ensuring safety and process efficiency. In this study, a novel electrochemical sensor based on the synergistic integration of MXene materials and deep eutectic solvents (DESs) was developed for the sensitive and stable detection of H_2O_2. MXenes, with their exceptional electrical conductivity and catalytic activity, serve as an efficient electrocatalytic platform, while DESs enhance their dispersion, stability, and electrochemical performance by preventing oxidation and aggregation. The resulting MXene-DES composite electrode exhibited a wide linear detection range (0.01-8.0 mM) and a low detection limit (1.5 μM). Moreover, the sensor demonstrated excellent reproducibility, long-term stability, and successful application in detecting H_2O_2 in real serum samples, underscoring its potential for clinical diagnostics and environmental monitoring. This study provides a green and efficient strategy for developing next-generation electrochemical sensors by combining advanced two-dimensional materials with environmentally benign solvent systems.

Keywords: Hydrogen peroxide, Electrochemical sensor, MXene, Deep eutectic solvent, Delamination.

Introduction

Hydrogen peroxide (H_2O_2) plays a crucial role as an oxidizing agent and disinfectant in a wide range of industrial and biomedical applications. Its applications span diverse fields including clinical diagnostics, pharmaceutical formulations, environmental monitoring, food safety, and agriculture. For instance, in medical diagnostics, H_2O_2 is involved in enzymatic reactions and oxidative stress processes, making it an important biomarker for disease states. In environmental science, its detection helps monitor water quality and pollutant degradation, while in food processing, it ensures microbial safety and extends shelf life. Due to its widespread application and potent chemical reactivity, precise and reliable measurement of H_2O_2 concentration is essential for maintain safety, optimizing processes, and comply with regulatory standards [1, 2]. Traditional analytical methods for detecting H_2O_2 such as, fluorescence spectroscopy [3, 4], and chromatographic techniques [5, 6] have provided effective tools for quantification. However, these methods often require costly instrumentation, extensive sample preparation, and skilled personnel, which can limit their applicability for rapid, on-site, or point-of-care testing [7]. In contrast, electrochemical sensing techniques have gained significant attention due to their inherent advantages of high sensitivity, selectivity, fast response times, and the possibility of miniaturization into portable devices [8, 9]. Electrochemical sensors convert the chemical

information generated by the analyte's redox reactions into measurable electrical signals, which can be precisely quantified. This feature makes them highly attractive for real-time monitoring in complex biological and environmental samples. MXenes, a relatively new class of two-dimensional (2D) transition metal carbides, nitrides, or carbonitrides, have demonstrated exceptional promise as electrode materials for electrochemical sensors [10, 11]. Their unique layered structure, combined with high electrical conductivity, hydrophilicity, and tunable surface chemistry, offers a versatile platform to enhance electron transfer kinetics and increase active surface area. These characteristics enable MXenes to act as highly efficient catalysts and conductive supports in sensor architectures [12, 13]. Nonetheless, MXenes suffer from inherent drawbacks that restrict their broader application. Specifically, their susceptibility to oxidation under ambient conditions and tendency to restack or agglomerate reduce the available active surface and deteriorate their electrochemical performance [14, 15]. Addressing these challenges is critical to unlock the full potential of MXenes in sensing technologies [16].

Deep eutectic solvents (DESs) have emerged as an innovative solution to improve the stability and dispersion of MXenes in sensor systems. DESs are eutectic mixtures composed of hydrogen bond donors and acceptors, which form a liquid phase at temperatures lower than those of their individual components [17-19]. Their remarkable properties include biodegradability, low toxicity, wide electrochemical windows, and tunable viscosity and conductivity. Importantly, DESs can provide a protective environment around MXene nanosheets, preventing oxidation and suppressing aggregation through strong intermolecular interactions [20, 21]. Moreover, the unique solvation environment in DESs facilitates enhanced mass transport and efficient electron transfer during electrochemical reactions. By incorporating DESs into MXene-based sensor platforms, it is possible to significantly improve sensor sensitivity, reproducibility, and long-term stability [22].

In the present study, the synergistic integration of MXene materials with DESs were explored to develop a novel electrochemical sensor for the sensitive and stable detection of H_2O_2. The sensor system benefits from the high catalytic activity and conductivity of MXenes, combined with the stabilizing and enhancing effects of DESs. The results showed that the proposed sensor achieves a broad linear detection range (0.01-8.0 mM) and a low detection limit (1.5 μm), which are critical parameters for practical analytical applications. Furthermore, the sensor's performance is validated by successful detection of H_2O_2 in real serum samples, illustrating its potential for clinical diagnostics and biomedical monitoring. This research highlights the promising direction of combining advanced 2D materials with green solvent systems to develop next-generation biosensors with improved functionality and sustainability.

Experimental:

Materials:

HF (48-50%), Choline Chloride (ChCl, ≥99%), and Urea (≥99%) were purchased, in analytical grade, from commercial sources (Sigma-Aldrich, Merck) and used as received, without any further purification. Ti_3AlC_2 (99.9%) and nickel foam was purchased from redox-kala. All aqueous solutions were prepared with doubly distilled water.

Morphological and topological characterizations of the electrode materials were conducted using a field emission scanning electron microscope (FESEM, MIRA3, TESCAN, Philips) operated at 20 kV. The crystallographic characteristics of the samples were obtained using a powder X-ray diffractometer (XRD, Philips X'pert diffractometer with CuK_α radiation (λ= 1.5406 Å) generated at 40 kV and 40 mA with a step size of 0.01 s^{-1}). All electrochemical studies were performed using a OrigaLys potentiostat/galvanostat (France) controlled via OrigaMaster 5 software. Surface area and pore size distribution were measured using a Micromeritics ASAP-2010 apparatus (at 77 K) from nitrogen adsorption/desorption isotherms by Brunauer-Emmett-Teller (BET) and Barrett-Joyner-Halenda (BJH) methods, respectively.

Synthesis of Ti_3C_2 MXene

To synthesize Ti_3C_2 MXene, 1 g of Ti_3AlC_2 MAX phase powder was gradually introduced into 20 mL of 50 wt% hydrofluoric acids under continuous stirring at ambient temperature [23]. The etching reaction was allowed to proceed for 24 hours to selectively remove the aluminum layers. Following the etching step, the obtained dispersion was repeatedly washed with deionized water and centrifuged several times until the pH approached neutrality (~6). The resulting solid product was then vacuum-dried at 60 °C to obtain multilayer Ti_3C_2 MXene powder suitable for subsequent applications.

Synthesis of DES

The DES was prepared by mixing a hydrogen bond donor (HBD) and a hydrogen bond acceptor (HBA) at an appropriate molar ratio. Typically, choline chloride

(ChCl) was used as the HBA and urea as the HBD in a 1:2 molar ratio [21]. The components were placed in a beaker and heated at 80 °C under constant magnetic stirring until a homogeneous, transparent liquid was formed. The resulting DES was allowed to cool the room temperature and stored in a sealed container to prevent moisture absorption prior to further use.

Synthesis DES-delaminated Ti_3C_2 MXene

The synthesis of DES-delaminated Ti_3C_2 MXene was adapted from a previously reported method with slight modifications [21]. For efficient delamination of Ti_3C_2 MXene layers, 1 mg of the as-prepared MXene powder was dispersed in 1 mL of methanol containing different concentrations of DES ranging from 0.1 to 0.5 wt/v%. The resulting suspension was subjected to ultrasonic treatment for 30 minutes at ambient temperature to promote layer separation and enhance dispersion stability. The following sonication, the mixture was centrifuged at 4000 rpm for 5 minutes, and the obtained sediment was thoroughly rinsed several times with methanol to eliminate any remaining DES residues. Finally, the cleaned product was oven-dried at 60 °C to obtain delaminated Ti_3C_2 MXene suitable for further characterization. According to previously published study [21], this intercalation not only promotes delamination and dispersion of the MXene sheets but also enables strong hydrogen-bonding interactions between the DES molecules and the MXene surface. Such interactions chemically passivate the Ti_3C_2 layers, effectively preventing oxidation and enhancing the structural stability of the hybrid composite.

Results and discussion:

Characteristic s of nanomaterials

The crystalline structures of Ti_3AlC_2 MAX phase, Ti_3C_2 MXene, and MXene-DES nanocomposites were characterized by XRD to confirm the successful synthesis and structural evolution after etching and surface modification. As shown in Figure 1, the diffraction pattern of Ti_3AlC_2 MAX phase exhibited strong and sharp characteristic peaks at 2θ = 10.1°, 20.3°, 36.6°, 38.7°, 41.9°, 44.7°, 48.1°, 51.8°, 55.7°, and 64.5°, corresponding to the (002), (004), (101), (103), (104), (105), (106), (107), (108), and (110) planes, respectively. These reflections are in good agreement with the standard JCPDS card (No. 52-0875) for Ti_3AlC_2, confirming the formation of a well-crystallized MAX phase with a layered hexagonal structure [24]. After selective etching of the Al layers using HF or an in-situ etching process, the resulting Ti_3C_2 MXene displayed a remarkable change in its XRD pattern. The characteristic (002) peak shifted significantly from 10.1° to about 8.57°, while other high-angle reflections such as (104) and (105) almost disappeared. This shift toward lower angles corresponds to an increase in interlayer spacing (d-spacing) from ~8.7 nm to ~1.02 nm, which confirms the successful removal of Al atoms and the formation of few-layered Ti_3C_2 MXene sheets. The broadening of the (002) peak further indicates partial exfoliation and decreased crystallinity due to the delamination of the MXene layers. For the MXene-DES composite, the XRD pattern maintained the typical (002) reflection of MXene but exhibited a further shift from 8.57° to about 6.56°, suggesting an additional expansion of the interlayer spacing (up to ~1.35 nm). This increase is attributed to the intercalation of DES molecules between the MXene layers, which prevents restacking and enhances the structural stability of the sheets. The reduced intensity and slight broadening of the (002) peak indicate the successful incorporation of DES components, leading to improved exfoliation and surface functionalization.

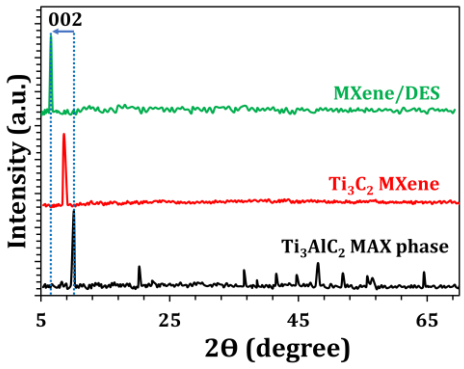

Fig. 1. XRD patterns of synthesized nanomaterials

The specific surface area and pore structure of the nanomaterials were investigated using nitrogen adsorption-desorption measurements based on the Brunauer-Emmett-Teller (BET) method (Figure 2A). The Ti_3AlC_2 MAX phase displayed a very low surface area of approximately 3.6 m^2 g^{-1}, due to its dense and compact layered structure in which Al layers are strongly bonded between Ti_3C_2 nanoshhets, limiting the accessible surface for gas adsorption. The Ti_3C_2 MXene exhibited a substantial increase in surface area to about 16.8 m^2 g^{-1}. This enhancement is attributed to the successful removal of Al atoms and the subsequent formation of open interlayer channels and few-layer nanosheets. Remarkably, the MXene-DES composite showed the highest BET surface area, reaching 42.4 m^2 g^{-1}. This significant increase is mainly due to the intercalation and stabilization effects of the DES, which prevents the restacking of MXene nanosheets

and creates additional interlayer voids. The incorporation of DES molecules between the MXene layers promotes delamination, enhances surface exposure, and maintains open channels for electrolyte diffusion. The surface morphology and microstructural evolution of Ti_3AlC_2 MAX phase, Ti_3C_2 MXene, and MXene-DES nanocomposites were characterized by FESEM, and the corresponding images are presented in Figures 2B to D. The Ti_3AlC_2 MAX phase (Figure 2B) exhibited a densely packed, layered structure with smooth and tightly stacked plate-like grains. The compact morphology and well-ordered lamellar arrangement are characteristic features of MAX phases, where strong metallic and covalent bonding between Ti, Al, and C atoms leads to a solid and rigid framework. Only limited interlayer gaps were observed, indicating that most surfaces are not accessible for ion or molecule penetration. After selective etching of the Al layers, the Ti_3C_2 MXene sample revealed a completely different morphology (Figure 2C). The FESEM image showed a distinct accordion-like or multilayered structure, confirming the successful removal of Al atoms and the formation of Ti_3C_2 nanosheets. The layers became more open and loosely stacked, providing abundant exposed surfaces and channels that are favorable for electrolyte diffusion and electron transport. In addition, slight surface roughness and nanoscale wrinkles were observed, which further enhance the active surface area. In the case of the MXene-DES composite, the morphology became even more delaminated and porous (Figure 2D). The MXene layers appeared thinner, more separated, and uniformly distributed, suggesting that the DES effectively intercalated between the MXene sheets and prevented their restacking. The DES molecules act as interlayer spacers and stabilizers, leading to the formation of a highly exfoliated, three-dimensional porous network structure. Such architecture not only increases the accessible electroactive area but also provides numerous transport pathways for ions and reactants, which is advantageous for electrochemical applications.

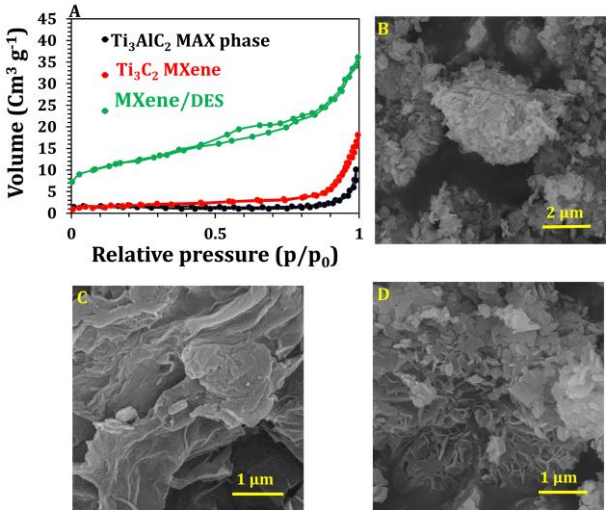

Fig. 2. (A) BET of the synthesis nanomaterials. FESEM images of Ti_3AlC_2 MAX phase (B), Ti_3C_2 MXene (C), and MXene-DES (D).

Electrochemical Response toward H_2O_2

The electrochemical behavior of different electrodes toward H_2O_2 was investigated by cyclic voltammetry (CV) in 0.1 M PB (pH 7.0) containing 0.2 mM H_2O_2. As shown in Figure 3A, distinct differences in the cathodic peak current were observed among the three electrodes. The bare GCE exhibited a weak and broad reduction peak with a current density of approximately 3.2 µA, indicating sluggish electron transfer and poor catalytic activity toward H_2O_2 reduction. Upon modification with MXene, the MXene/GCE electrode showed a significantly enhanced reduction peak current of about 11.4 µA, corresponding to an increase of nearly 3.6 times compared with the bare GCE. This enhancement arises from the high electrical conductivity, large surface area, and abundant surface functional groups of MXene that facilitate electron transfer. Interestingly, the MXene-DES/GCE electrode exhibited the highest electrocatalytic activity, with a cathodic peak current reaching 22.8 µA, which is about 7.1 times higher than that of the bare GCE and roughly 2 times greater than the MXene/GCE electrode. In addition, the reduction potential shifted positively from -0.98 V (bare GCE) to -0.87 V (MXene/GCE) and further to -0.84 V (MXene-DES/GCE), suggesting that the reaction kinetics were significantly improved. The enhanced performance of MXene-DES/GCE can be attributed to the synergistic effect between MXene and the DES, which improves the dispersion and stability of MXene nanosheets, increases the number of electroactive sites, and facilitates rapid electron transfer. Therefore, MXene-DES/GCE demonstrates outstanding electrocatalytic performance and holds great promise for sensitive electrochemical detection of H_2O_2.

Optimization of DES Content

To achieve the best electrochemical performance, the effect of the amount of DES used during the modification of MXene was systematically investigated. A series of MXene-DES composites with different DES contents

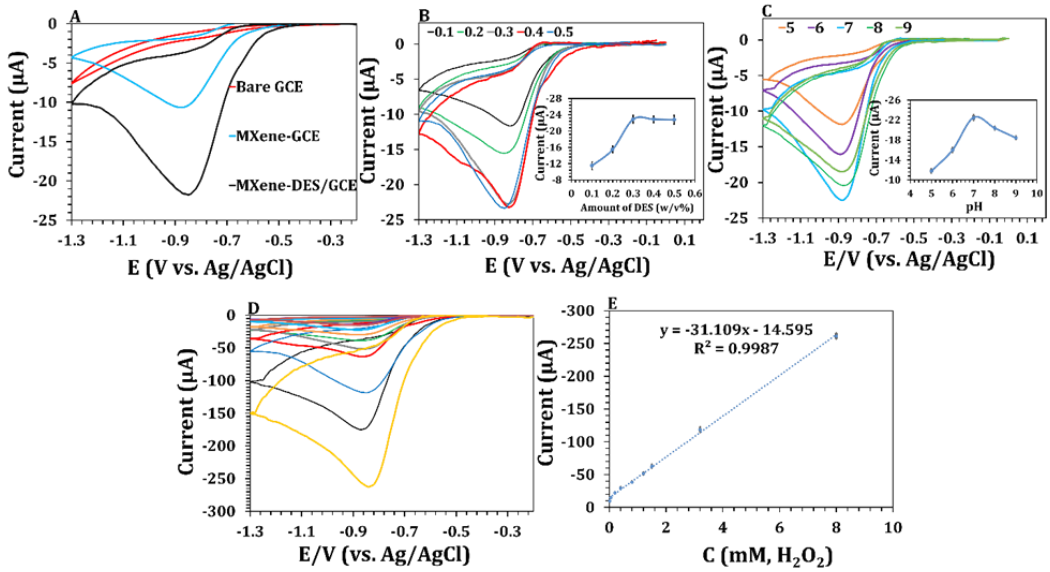

Fig. 3. (A) Electrochemical behavior of different electrodes toward H_2O_2 in 0.1 M PB (pH 7.0) containing 0.2 mM H_2O_2. (B) The effect of the amount of DES (0.1, 0.2, 0.3, 0.4, 0.5 w/v%) on electrocatalytic reduction of H_2O_2. (C) Effect of solution pH (5–9) on the response of MXene-DES/GCE in 0.1 M PB (pH 7.0) containing 0.2 mM H_2O_2. (D) Electroreduction of the MXene-DES/GCE in the presence of varying H_2O_2 concentrations (0.01, 0.05, 0.2, 0.4, 0.8, 1.2, 1.5, 3.2, 8 mM) under optimum conditions. (E) The corresponding calibration curve obtained from the data in (D), showing the linear response range of the electrode.

.

(0.1%, 0.2%, 0.3%, 0.4%, and 0.5% w/v) were prepared and drop-cast onto the GCE surface under identical conditions. The corresponding CVs were recorded in 0.1 M PBS containing 0.2 mM H_2O_2. As shown in Figure 3B, the cathodic peak current increased gradually with increasing DES content up to 0.3%, indicating that a moderate amount of DES effectively enhanced the dispersion and stabilization of MXene nanosheets on the electrode surface. This optimal composition promoted the formation of a uniform and conductive network with abundant accessible active sites for the reduction of H_2O_2. However, when the DES content exceeded 0.3%, a gradual decline in the peak current was observed. The decrease can be attributed to the excessive amount of DES, which may lead to partial aggregation of MXene sheets or the formation of a thicker and less conductive film that hinders electron transfer between MXene and the electrode substrate.

Optimization of pH conditions

The influence of solution pH on the electrochemical response toward hydrogen peroxide was systematically investigated to determine the optimal operating conditions. 0.1 M PB with pH values ranging from 5.0 to 9.0 were prepared and employed as the electrolyte (Figure 3C). The electrochemical behavior of the MXene-DES modified electrode was evaluated by measuring the current response of H_2O_2 under identical experimental parameters. It was observed that the sensor response gradually increased with increasing pH up to a certain point and then declined at higher values, indicating that the proton concentration strongly affects the redox kinetics of hydrogen peroxide. The maximum current signal was obtained at pH 7.0, suggesting that neutral conditions provide the most favorable environment for efficient electron transfer and catalytic activity. Therefore, subsequent electrochemical measurements were performed at pH 7.0 to ensure optimal sensor performance.

Analytical Performance of the MXene-DES/GCE electrode toward H_2O_2

The analytical performance of the MXene-DES/GCE electrode for hydrogen peroxide detection was evaluated by measuring the cathodic peak current at various H_2O_2 concentrations under optimized conditions. CV measurements were performed in 0.1 M PBS (pH 7.0), with various concentrations of H_2O_2. As illustrated in Figure 3D and E, the cathodic peak current increased linearly with H_2O_2 concentration in the range of 0.01-8.0 mM, demonstrating that the electrode response is directly proportional to the analyte concentration. The limit of detection (LOD) was calculated based on a signal-to-noise ratio of 3, resulting in LOD=0.15 µM, highlighting the high sensitivity of the MXene-DES/GCE. These results confirm that the MXene-DES/GCE electrode

provides a reliable and sensitive platform for quantitative determination of hydrogen peroxide over a wide concentration range, making it suitable for analytical applications in environmental and biological samples.

Effect of Scan Rate

The influence of the scan rate on the electrochemical response of the MXene-DES/GCE toward H_2O_2 (0.5 mM H_2O_2 in 0.1 M PBS, pH 7.0) was systematically investigated using cyclic voltammetry. CVs were recorded at scan rates ranging from 10 to 250 mV s^{-1}. As shown in Figure 4A, the cathodic peak current (I_p) increased with increasing scan rate, indicating that the electrode reaction is dependent on the rate of electron transfer. A linear relationship was observed between I_p and the square root of the scan rate ($\nu^{1/2}$) (Figure 4B). This linearity suggests that the reduction of H_2O_2 on MXene-DES/GCE is a diffusion-controlled process, where the mass transport of H_2O_2 to the electrode surface governs the current response.

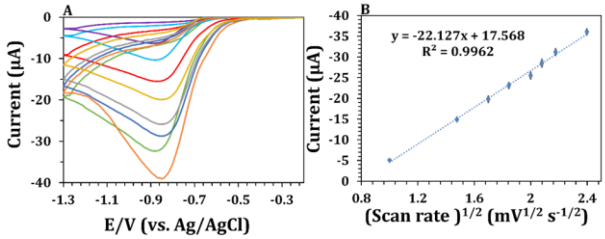

Fig. 4. (A) The influence of the scan rate on the electrochemical response of the MXene-DES/GCE toward H_2O_2 (0.5 mM H_2O_2 in 0.1 M PBS, pH 7.0). (B) A linear relationship between I_p and the square root of the scan rate ($\nu^{1/2}$).

Investigation of stability, Repeatability, Reproducibility, and Selectivity

The electrochemical stability tests were performed in 0.1 M PB (pH 7.0) containing 0.5 mM H_2O_2 (Figure 5A). After storage under dry conditions at room temperature for two weeks, the electrode retained about 96% of its initial current response, demonstrating outstanding durability and structural integrity. This excellent stability originates from the strong interfacial interactions between MXene nanosheets and DES molecules, which effectively prevent oxidation, restacking, and structural degradation of the MXene layers over time. To assess repeatability, five consecutive measurements were conducted under identical conditions, yielding an RSD of 2.8%, confirming excellent operational consistency (Figure 5B). Furthermore, reproducibility was verified by using five independently prepared electrodes, which exhibited an RSD of 3.1%, indicating reliable fabrication and uniform electrocatalytic activity across electrodes (Figure 5C). These findings demonstrate that DES modification not only enhances electrocatalytic performance but also ensures stable and reproducible electrode behavior. The selectivity of the MXene-DES/GCE electrode was also examined in the presence of common interferents such as glucose (Glu), ascorbic acid (AA), uric acid (UA), and dopamine (DA) (each at concentrations ten times higher than that of H_2O_2) (Figure 5D). No measurable current response was observed for these species, and their presence did not affect the cathodic peak current of H_2O_2. This issue confirms that the electrode exhibits excellent anti-interference ability and high selectivity, attributed to the synergistic interaction between MXene nanosheets and DES molecules that promotes selective electron transfer toward H_2O_2 while suppressing non-specific adsorption and side reactions.

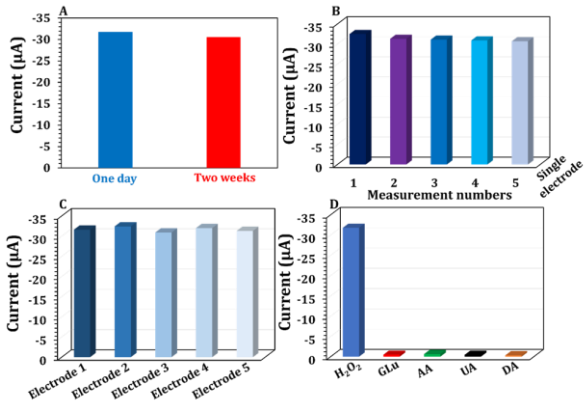

Fig. 5. (A) The stability of the MXene/DES-GCE for two weeks by keeping the modified GCE in a PB (0.1 M, pH=7.0). The repeatability (B) and the reproducibility (C) of the modified GCE. (D) Selectivity of the MXene/DES-GCE toward 0.5 mM H_2O_2 against common interferences at tenfold higher concentrations.

Real Sample Analysis

The practical applicability of the MXene-DES/GCE electrode was verified by detecting hydrogen peroxide in human serum samples. Before measurement, the serum was diluted with 0.1 M PB (pH 7.0) to minimize matrix effects. Electrochemical measurements were performed using the standard addition method. As summarized in Table 1, the electrode exhibited high recovery rates (95.0–102.5%) with RSD values below 4%, demonstrating reliable and accurate detection of H_2O_2 in complex biological matrices. The superior performance is attributed to the high electrocatalytic activity, and large surface area of the MXene-DES composite, which facilitate efficient electron transfer and maintain accessibility of active sites even in the serum environment. Overall, these results confirm that the MXene-DES/GCE electrode provides a robust, sensitive,

and reproducible sensing platform suitable for biomedical and clinical applications involving hydrogen peroxide detection.

Table 1. Determination of H_2O_2 in Human Serum Samples Using MXene-DES/GCE Electrode

Sample	Added H_2O_2 (mM)	Found H_2O_2 (mM)	Recovery (%)	RSD (%)
Human serum	0.2	0.19	95.0	3.1
	0.5	0.49	98.0	2.9
	1.0	1.02	102.0	3.3
	2.0	2.05	102.5	3.5
	5.0	5.10	102.0	3.8

Conclusion

In summary, a highly sensitive and stable electrochemical sensor for hydrogen peroxide detection was successfully fabricated by integrating MXene materials with deep eutectic solvents (DESs). The synergistic combination of MXenes' outstanding electrical conductivity and catalytic activity with the stabilizing and dispersing capabilities of DESs significantly enhanced the electrochemical performance of the sensor. The developed MXene-DES composite electrode exhibited a broad linear detection range (0.01-8.0 mM), a low detection limit (1.5 μM), and excellent reproducibility and long-term operational stability. Furthermore, its successful application in real serum samples demonstrates the feasibility of this sensor for practical biomedical and environmental analyses. This study provides valuable insight into the design of next-generation, green electrochemical sensors by leveraging the complementary advantages of two-dimensional materials and environmentally benign solvent systems. The present approach can be further extended to the development of sustainable sensing platforms for diverse analytes in clinical, environmental, and industrial settings. Table 2 compares the analytical performance of the proposed DES-delaminated Ti_3C_2 MXene-based electrode with previously reported electrochemical sensors for hydrogen peroxide. Although some reported sensors show comparable or even superior analytical parameters, such as lower detection limits or wider linear ranges, many of them require complicated electrode fabrication or multistep modification procedures. In contrast, the present sensor benefits from a simple and straightforward fabrication strategy while still delivering reliable analytical performance, making it attractive for practical and routine applications.

Table 2. Comparison of the analytical performance of the proposed DES-delaminated Ti_3C_2 MXene-based electrode with previously reported electrochemical sensors for hydrogen peroxide detection.

Electroactive material	Linearity (mM)	LOD (μM)	Ref.
Anti-CEA/AuNPs/PB-MXene	0.001-0.5	0.57	25
Gr/PtAuNC-$C6_{His16}$	0.05-10	0.6	26
Cells/GelMA/CNF/MNO_2NW/AuNPs	0.05-0.1	2	27
3D Ni-graphene@au skeletons	0.1-1.0	33.5	28
AuNFs/(PEI/PAA)10/GR	0.005-5	4.5	29
rGO/AuNPs	0.025-3	6.55	30
ITO-PET			
Cu-PAM	0.05-25.31	0.16	31
Ce–hemin–MOFs/GO	0.01-10	1.2	32
HRP-$Cu_3(PO_4)_2$	0.1–50	1.8	33
MXene-DES	0.01-8	1.5	This work

References

[1] S. Ma, S. Xiao, Y. Hong, Y. Bao, Z. Xu, D. Chen, X. Huang, Coupling metal organic frameworks nanozyme with carbon nanotubes on the gradient porous hollow fiber membrane for nonenzymatic electrochemical H_2O_2 detection, ***Analytica Chimica Acta*** **2024**, 1293, 342285. https://doi.org/https://doi.org/10.1016/j.aca.2024.342285.

[2] L. Wang, J. Shi, P. Wang, R. Rong, High-sensitive detection of H_2O_2 in biological systems by persistent luminescent nanoprobes, ***Chemical Engineering Journal*** **2024**, 486, 150291. https://doi.org/https://doi.org/10.1016/j.cej.2024.150291.

[3] L. Peng, H. Guo, N. Wu, M. Wang, Y. Hui, H. Ren, B. Ren, W. Yang, Fluorescent sensor based on bismuth metal-organic frameworks (Bi-MOFs) mimic enzyme for H_2O_2 detection in real samples and distinction of phenylenediamine isomers, ***Talanta*** **2024**, 272, 125753. https://doi.org/https://doi.org/10.1016/j.talanta.2024.125753.

[4] H. Dong, L. Zheng, Z. Wang, K. Xu, W. Chen, Z. Liu, Z. Chang, Y. Zhou, X. Zhu, Y. Zhang, Dual-mode ratiometric electrochemical and turn-on fluorescent probe for reliably detecting H_2O_2 in Parkinson's disease serum, ***Sensors and Actuators Reports*** **2025**, 9, 100305. https://doi.org/https://doi.org/10.1016/j.snr.2025.100305.

[5] J. Park, H. Noh, H.J. Suh, D. Ryu, H.J. Lee, C. Lee, High-performance liquid chromatography using diode array detector and fluorescence detector for hydrogen peroxide analysis in processed fishery foods, ***Food Science and Biotechnology*** **2023**, 32, 27-37. https://doi.org/10.1007/s10068-022-01165-1.

[6] M. Tarvin, B. McCord, K. Mount, M.L. Miller, Analysis of hydrogen peroxide field samples by HPLC/FD and HPLC/ED in DC mode, ***Forensic Science International*** **2011**, 209, 166-72. https://doi.org/10.1016/j.forsciint.2011.01.024.

[7] J. Liu, M. Li, W. Liu, Z. Hao, F. Zhang, H. Pang, R. Zhang, L. Zhang, Advances in non-enzymatic electrochemical materials for H_2O_2 sensing, ***Journal of Electroanalytical Chemistry*** **2024**, 954, 118060. https://doi.org/https://doi.org/10.1016/j.jelechem.2024.118060.

[8] Y. Liu, C. Wang, Y. Zhang, X. Zeng, J. Li, M. Yang, D. Huo, C. Hou, A flexible self-supported electrochemical sensor Co-NC/PS@ CC for real-time detection of cell-released H_2O_2, ***Analytica Chimica Acta*** **2024**, 1307, 342627. https://doi.org/https://doi.org/10.1016/j.aca.2024.342627.

[9] D. Mohanapriya, K. Thenmozhi, In situ developed $NiCo_2O_4$–$Ti_3C_2T_x$ nanohybrid towards non-enzymatic electrochemical detection of glucose and hydrogen peroxide, ***Journal of Materials Chemistry B*** **2025**, 13, 2306-2316. https://doi.org/https://doi.org/10.1039/D4TB02265C.

[10] R. Kumar, L. Singh, $Ti_3C_2T_x$ MXene as Electrocatalyst for Designing Robust Glucose Biosensors, ***Advanced Materials Technologies*** **2022**, 7, 2200151. https://doi.org/https://doi.org/10.1002/admt.202200151.

[11] C. Tsounis, P.V. Kumar, H. Masood, R.P. Kulkarni, G.S. Gautam, C.R. Müller, R. Amal, D.A. Kuznetsov, Advancing MXene Electrocatalysts for Energy Conversion Reactions: Surface, Stoichiometry, and Stability, ***Angewandte Chemie International Edition*** **2023**, 62, e202210828. https://doi.org/https://doi.org/10.1002/anie.202210828.

[12] S.K. Bhardwaj, H. Singh, M. Khatri, K.-H. Kim, N. Bhardwaj, Advances in MXenes-based optical biosensors: A review, ***Biosensors & Bioelectronics*** **2022**, 202, 113995. https://doi.org/https://doi.org/10.1016/j.bios.2022.113995.

[13] S.M. Khoshfetrat, M. Nabavi, S. Mamivand, Z. Wang, Z. Wang, M. Hosseini, Ionic liquid-delaminated Ti_3C_2 MXene nanosheets for enhanced electrocatalytic oxidation of tryptophane in normal and breast cancer serum, ***Mikrochimica Acta*** **2025**, 192, 113. https://doi.org/10.1007/s00604-025-06968-7.

[14] S.M. Khoshfetrat, M. Motahari, S. Mirsian, 3D porous structure of ionic liquid-delaminated Ti_3C_2 MXene nanosheets for enhanced electrochemical sensing of tryptophan in real samples, ***Scientific Reports*** **2025**, 15, 6804. https://doi.org/10.1038/s41598-025-91773-8.

[15] S.M. Khoshfetrat, In situ synthesis of nickel-substituted zeolitic metal-organic framework on Ti_3C_2 MXene for enhanced electrocatalytic sensing of L-tryptophan, ***Journal of Electroanalytical Chemistry*** **2025**, 119215. https://doi.org/10.1016/j.jelechem.2025.119215.

[16] L. Liu, Z. Yang, J. Zhang, L. Wang, J. Pang, A. Wang, L. Ding, H. Liu, X. Yu, Research progress in the application of MXene in bacterial detection and eradication, ***Materials Today Physics*** **2024**, 43, 101412. https://doi.org/https://doi.org/10.1016/j.mtphys.2024.101412.

[17] Q. Salamat, J.P.C. Brandão, A. de Freitas Santos Junior, M. Soylak, Deep eutectic solvent-based ferrofluids: Synthesis strategies, characteristics, and applications for trace analytes extraction, ***TrAC, Trends in Analytical Chemistry*** **2025**, 184, 118126. https://doi.org/https://doi.org/10.1016/j.trac.2024.118126.

[18] Y. Nie, Y. Zhou, Y. Zhang, D. Sun, D. Wu, L. Ban, S. Nanda, C. Xu, H. Zhang, Sustainable Synthesis of Functional Materials Assisted by Deep Eutectic Solvents for Biomedical, Environmental, and Energy Applications, ***Advanced Functional Materials*** **2025**, 35, 2418957. https://doi.org/10.1002/adfm.202418957.

[19] E.L. Smith, A.P. Abbott, K.S. Ryder, Deep Eutectic Solvents (DESs) and Their Applications, ***Chemical Reviews*** **2014**, 114, 11060-11082. https://doi.org/10.1021/cr300162p.

[20] T. Li, Y. Chen, Z. Han, J. Wang, X. Li, L. Zhang, Y. Yu, Deep Eutectic Solvent-Modified MXene as Nonpolar Lubricant Additives, ***ACS Applied Nano Materials*** **2025**, 8, 4470-4483. https://doi.org/10.1021/acsanm.4c06785.

[21] J. Kim, Y. Yoon, S.K. Kim, S. Park, W. Song, S. Myung, H.-K. Jung, S.S. Lee, D.H. Yoon, K.-S. An, Chemically Stabilized and Functionalized 2D-MXene with Deep Eutectic Solvents as Versatile Dispersion Medium, ***Advanced Functional Materials*** **2021**, 31, 2008722. *https://doi.org/10.1002/adfm.202008722*.

[22] P. Cao, J. Feng, T. Yang, H. Ao, T. Shang, B. Xing, MXene-enhanced deep eutectic solvent-based flexible strain sensor with high conductivity and anti-freezing using electrohydrodynamic direct-writing method, ***Colloids and Surfaces A: Physicochemical and Engineering Aspects*** **2023**, 677, 132349. https://doi.org/10.1016/j.colsurfa.2023.132349.

[23] B. Wang, S.M. Khoshfetrat, H. Mohamadimanesh, Peroxidase-like manganese oxide nanoflowers-delaminated Ti_3C_2 MXene for ultrasensitive dual-mode and real-time detection of H2O2 released from cancer cells, ***Microchemica Journal*** **2024**, 207, 111796. https://doi.org/10.1016/j.microc.2024.111796.

[24] W. Wang, Z. Ma, Q. Shao, J. Wang, L. Wu, X. Huang, Z. Hu, N. Jiang, J. Dai, L. He, Multi-MXene assisted large-scale manufacturing of electrochemical biosensors based on enzyme-nanoflower enhanced electrodes for the detection of H_2O_2 secreted from live cancer cells, ***Nanoscale*** **2024**, 16, 12586-12598. https://doi.org/10.1039/D4NR01328J.

[25] X. Su, Q. You, L. Zhuang, Z. Chang, M. Ge, L. Yang, W.-F. Dong, Bifunctional electrochemical biosensor based on PB-MXene films for the real-time analysis and detection of living cancer cells, ***Journal of Pharmaceutical and Biomedical Analysis*** **2023,** 234, 115479-115485. https://doi.org/10.1016/j.jpba.2023.115479

[26] A. Silvestri, S. Vázquez-Díaz, G. Misia, F. Poletti, R. López-Domene, V. Pavlov, C. Zanardi, A.L. Cortajarena, M. Prato, An Electroactive and Self-Assembling Bio-Ink, based on Protein-Stabilized Nanoclusters and Graphene, for the Manufacture of Fully Inkjet-Printed Paper-Based Analytical Devices, ***Small*** **2023**, 19(51), 2300163-2300172. https://doi.org/10.1002/smll.202300163.

[27] Y. Ye, X. Sun, Y. Zhang, X. Han, X. Sun, A novel cell-based electrochemical biosensor based on MnO_2 catalysis for antioxidant activity evaluation of anthocyanins, ***Biosensors & Bioelectronics*** **2022**, 202,

113990-113998. https://doi.org/10.1016/j.bios.2022.113990.

[28] H.-W. Chang, Y.-H. Chen, J.-Y. Lin, Visible light-assisted photoelectrochemical sensing platforms based on the hierarchical architectures of 3D Ni-graphene@au skeletons for H_2O_2 detection in human serum, ***Journal of Electroanalytical Chemistry*** **2025**, 998, 119523-119531. https://doi.org/10.1016/j.jelechem.2025.119523.

[29] L. Zhang, Y. Wang, Y. Wang, M. Guo, Z. Li, X. Jin, H. Du, Electrochemical H_2O_2 sensor based on a Au nanoflower-graphene composite for anticancer drug evaluation, ***Talanta*** **2023**, 261, 124600-124610. https://doi.org/10.1016/j.talanta.2023.124600.

[30] B. Patella, M. Buscetta, S. Di Vincenzo, M. Ferraro, G. Aiello, C. Sunseri, E. Pace, R. Inguanta, C. Cipollina, Electrochemical sensor based on rGO/Au nanoparticles for monitoring H_2O_2 released by human macrophages, ***Sensors & Actuators, B: Chemical*** **2021**, 327, 128901-128911. https://doi.org/10.1016/j.snb.2020.128901.

[31] L. Su, Y. Li, H. Chen, X. Liu, Z. Zhang, D. Bin, B. Yang, L. Sun, H. Lu, B. Liu, Polyacrylamide-incorporated copper electrodes for electrochemical-colorimetric dual-mode detection of H_2O_2 released from tomato leaves, ***Talanta*** **2025**, 287, 127689-127698. https://doi.org/10.1016/j.talanta.2025.127689.

[32] H. Ghaedamini, R. Khanal, D.-S. Kim, Peroxidase-mimicking Ce-hemin–MOFs/GO composite for enzyme-free electrochemical detection of H_2O_2, ***Journal of Electroanalytical Chemistry*** **2026**, 1002, 119744-119757. https://doi.org/10.1016/j.jelechem.2025.119744.

[33] M. Luo, Y. Song, N. Ali Khan, W. Wei, Y. Lu, Q. Zhao, H. Jiang, M. Li, D. Wang, Facile fabrication of HRP-$Cu_3(PO_4)_2$ hybrid nanoflowers on screen-printed electrode for electrochemical detection of H_2O_2, ***Microchemical Journal*** **2024,** 197, 109845-109855. https://doi.org/10.1016/j.microc.2023.109845.